Synthesis of Near-Infrared-Absorbing Nanoparticle-Assembled Capsules

Jie Yu,[†] Mohammad A. Yaseen,[‡] Bahman Anvari,[‡,§] and Michael S. Wong*[,†,#]

Departments of Chemical and Biomolecular Engineering, Bioengineering, and Chemistry, Rice University, Houston, Texas 77005

Received September 1, 2006. Revised Manuscript Received December 26, 2006

Indocyanine green (ICG) is an FDA-approved photosensitizer dye used in clinical settings for optical diagnostics and near-infrared laser-based therapy. However, the rapid clearance and nonspecific vascular plasma binding issues impede ICG performance. Encapsulating ICG within a colloidal matrix is a potential approach to solving these problems, but thus far, there has been limited success. A new strategy, based on the nanoparticle assembly synthesis of stable, non-liposomal nanoparticle/polymer microcapsules, to encapsulate ICG is presented. Nanoparticle-assembled capsules (NACs) are prepared at room temperature, in aqueous solution, and at neutral pH by combining a polyallylamine solution, a phosphate solution, and an aqueous sol of silica nanoparticles; ICG-containing NACs with 0.6−1.0 μm diameter are prepared by adding an ICG solution before the nanoparticle sol. ICG loading is readily controlled with an attainable maximum loading of ∼23 wt %. There is negligible leakage from the capsules after 24 h at room temperature in phosphate buffer saline solution, with 17% ICG leakage after 8 h at 37 °C. ICG-containing NACs are capable of heat generation in response to near-infrared laser irradiation and are stable to multiple photothermal heating cycles. Fibroblast cells exposed to these capsules remain viable after 2 days of incubation. ICG-containing NACs are a promising material for new photothermal therapy applications and are illustrative of a new approach for encapsulating organic dye compounds.

Introduction

Indocyanine green (ICG) is an amphiphilic carbocyanine dye (molecular weight = 775.0, CAS no. 3599-32-4) that strongly absorbs and fluoresces in the near-infrared region of light (NIR, 740−3000 nm), exhibiting absorption and emission maxima at ∼780 and ∼820 nm, respectively.[1,2] Conveniently, human tissues have low absorption in the NIR compared to other spectral regions.[3] With low toxicity (semilethal dose LD_{50} of 50−80 mg/kg for animal subjects[4]) and U.S. Food and Drug Administration (FDA) approval for clinical use, ICG is used as a contrast agent to optically image the human vasculature for medical diagnostic applications (e.g., retinal angiography since the 1970s).[2,5−12] ICG has also been studied as a basis for medical treatment. It can convert the absorbed light energy to produce heat and toxic chemical species (such as singlet oxygen, superoxide anions, and hydroxyl radicals), forming the respective bases for photothermal[13,14] and photodynamic therapies.[13,15−18] Specific applications under investigation include laser tissue welding[19,20] and treatment of skin diseases[13,17] and cancers.[14−16,21]

There are several problems that limit the development of ICG for new phototherapy applications. First, its pharmacokinetics is extremely fast; ICG clears rapidly from the circulatory system with a half-life of 3−4 min, followed by a much slower clearance rate characterized by a half-life of 1+ h.[10] Second, ICG has complicated solution behavior due

* Corresponding author. E-mail: mswong@rice.edu.
[†] Department of Chemical and Biomolecular Engineering, Rice University.
[‡] Department of Bioengineering, Rice University.
[§] Current address: Department of Bioengineering, University of California, Riverside, CA.
[#] Department of Chemistry, Rice University.

(1) Landsman, M. L. J.; Kwant, G.; Mook, G. A.; Zijlstra, W. G. *J. Appl. Physiol.* **1976**, *40*, 575−583.
(2) Benson, R. C.; Kues, H. A. *Phys. Med. Biol.* **1978**, *23*, 159−163.
(3) Bashkatov, A. N.; Genina, E. A.; Kochubey, V. I.; Tuchin, V. V. *J. Phys. D* **2005**, *38*, 2543−2555.
(4) Taichman, G. C.; Hendry, P. J.; Keon, W. J. *Tex. Heart Inst. J.* **1987**, *14*, 133−138.
(5) Lund-Johansen, P. *Eur. Heart J.* **1990**, *11*, 6.
(6) Dorshow, P. B.; Bugaj, J. E.; Burleigh, B. D.; Duncan, J. R.; Johnson, M. A.; Joes, W. B. *J. Biomed. Opt.* **1998**, *3*, 340.
(7) Maarek, J. M. I.; Holschneider, D. P.; Harimoto, J.; Yang, J.; Scremin, O. U.; Rubinstein, E. H. *Anesthesiology* **2004**, *100*, 1476−1483.
(8) Maarek, J. M. I.; Holschneider, D. P.; Yang, J.; Pniak, S. N.; Rubinstein, E. H. *Anesthesiology* **2005**, *102*, 774−782.
(9) Kim, D. E.; Jaffer, F. A.; Weissleder, R.; Tung, C. H.; Schellingerhout, D. *J. Cereb. Blood Flow Metab.* **2005**, *25*, 226−233.
(10) Desmettre, T. D.; J. M.; Mordon, S. *Surv. Ophthalmal.* **2000**, *45*, 15−27.
(11) Intes, X.; Ripoll, J.; Chen, Y.; Nioka, S.; Yodh, A. G.; Chance, B. *Med. Phys.* **2003**, *30*, 1039−1047.
(12) Hawrysz, D. J.; Sevick-Muraca, E. M. *Neoplasia* **2000**, *2*, 388−417.
(13) Tuchin, V. V.; Genina, E. A.; Bashkatov, A. N.; Simonenko, G. V.; Odoevskaya, O. D.; Altshuler, G. B. *Lasers Surg. Med.* **2003**, *33*, 296−310.
(14) Chen, W. R.; Adams, R. L.; Bartels, K. E.; Nordquist, R. E. *Cancer Lett.* **1996**, *98*, 169−173.
(15) Urbanska, K.; Romanowska-Dixon, B.; Matuszak, Z.; Oszajca, J.; Nowak-Sliwinska, P.; Stochel, G. *Acta Biochim. Pol.* **2002**, *49*, 387−391.
(16) Baumler, W.; Abels, C.; Karrer, S.; Weiss, T.; Messmann, H.; Landthaler, M.; Szeimies, R. M. *Brit. J. Cancer* **1999**, *80*, 300−363.
(17) Genina, E. A.; Bashkatov, A. N.; Simonenko, G. V.; Odoevskaya, O. D.; Tuchin, V. V.; Altshuler, G. B. *J. Biomed. Opt.* **2004**, *9*, 828−834.
(18) Abels, C.; Karrer, S.; Baumler, W.; Goetz, A. E.; Landthaler, M.; Szeimies, R-M. *Brit. J. Cancer* **1998**, *77*, 1021−1024.
(19) Wolfe, J. D.; Csaky, K. G. *Exp. Eye Res.* **2004**, *79*, 631−638.
(20) Desmettre, T.; Soulie-Begu, S.; Devoisselle, J. M.; Mordon, S. *Invest. Ophthalmol. Vis. Sci.* **1999**, *40*, S321−S321.
(21) Chen, W. R.; Adams, R. L.; Bartels, K. E.; Nordquist, R. E. *Cancer Lett.* **1995**, *94*, 125−131.

10.1021/cm062080x CCC: $37.00
Published on Web 02/21/2007

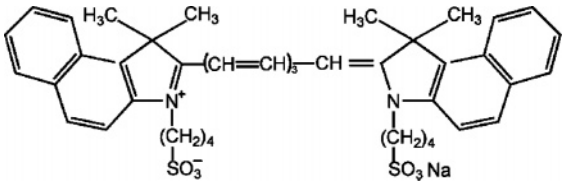

Figure 1. Molecular structure of ICG.

to its amphiphilic nature (hydrophilic sulfate groups and hydrophobic dimethylated benzoindotricarbocyanin groups, Figure 1). It forms aggregates in water depending on its concentration (bathochromically shifting its absorbance characteristics and reducing fluorescence quantum efficiency[22]) and binds nonspecifically to human serum albumin, lipoproteins, plasma proteins, and endothelial cells.[23,24] Third, an aqueous ICG solution is unstable, as the compound undergoes thermal degradation and photodegradation.[10,22,25−28] The nonfluorescent degradation products are thought to be polycyclic fragments, partially hydrogenated ICG, or ICG with a new ring structure.

The preparation of colloidal carriers for ICG has been studied to address the issues of fast blood clearance and uncontrolled protein binding. Emulsions, like a phospholipid-stabilized oil-in-water system[29,30] and a lecithin-stabilized commercial product called Intralipid,[31] are one such material. Devoisselle et al. reported that blood clearance time was lengthened but that the instability of the emulsion structure led to ICG leakage.[29] Polymeric particles have recently been studied as another ICG carrier. Saxena et al. prepared ∼300 nm poly(lactic-co-glycolic acid) (PLGA) particles that contained ICG (as much as 29 wt %).[32−34] ICG chemical stability was increased and clearance time was lengthened; the leakage rate was quite significant, though (78% loss over 8 h at 37 °C in phosphate-buffered saline solution, pH 7.4).[32] Polymeric capsules containing NIR-responsive dyes or NPs can be prepared through a technique called layer-by-layer assembly.[35−41] The salient features are the multiple steps in their preparation and encapsulation, and capsule deformation upon drying due to their thin shells (tens of nanometers).

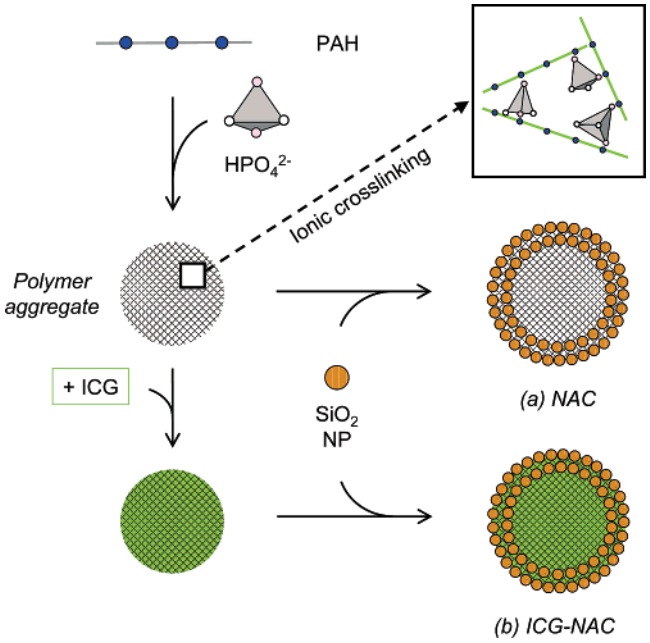

Figure 2. Formation mechanism schematic for (a) nanoparticle-assembled capsules (NACs) and (b) ICG-containing NACs (ICG-NACs).

Here, we report on nanoparticle-assembled capsules (NACs) as a new type of delivery vehicle for ICG. NACs are synthesized through a two-step NP assembly process.[42−44] In the first step, positively charged polymer chains and multivalence anions are combined to form ionically cross-linked polymer aggregates, and in the second step, negatively charged SiO_2 NPs are combined with the aggregates to form the capsules (Figure 2a). The shell is composed of NPs and polymer, and the core interior contains the polymer aggregate. NAC formation occurs rapidly (on the order of seconds) and the conditions are very mild (at room temperature, in aqueous solution, and at neutral pH). From an implementation point-of-view, NP assembly of capsules is simpler to carry out than layer-by-layer assembly. NAC synthesis is highly suitable as an encapsulation method, particularly for a charged molecule like ICG. We describe the successful synthesis of ICG-containing NACs and the conditions that lead to ICG content control and discuss leakage, cell toxicity, and photothermal results that are indicative of a promising new phototherapeutic material.

Experimental Section

Materials. Poly(allylamine hydrochloride) ("PAH," 70 000 g/mol, chloride counterion, Sigma-Aldrich), disodium hydrogen phosphate heptahydrate ($Na_2HPO_4{\cdot}7H_2O$, 99.5%, Fisher), and

(22) Zhou, J. F.; Chin, M. P.; Schafe, S. A. In *Laser Surgery: Advanced Characterization, Therapeutics and Systems IV*; Anderson, R., Ed.; SPIE: Bellingham, WA, 1994; Vol. IV, p 495.
(23) Patonay, G.; Salon, J.; Sowell, J.; Strekowski, L. *Molecules* **2004**, *9*, 40−49.
(24) Mordon, S.; Devoisselle, J. M.; Soulie-Begu, S.; Desmettre, T. *Microvasc. Res.* **1998**, *55*, 146−152.
(25) Gathje, J.; Steuer, R. R.; Nicholes, K. R. *J. Appl. Phys.* **1970**, *29*, 181−185.
(26) Barbier, F.; Deweerdt, G. A. *Clin. Chim. Acta* **1964**, *10*, 549.
(27) Gratz, H.; Penzkofer, A.; Abels, C.; Szeimies, R. M.; Landthaler, M.; Baumler, W. *J. Photochem. Photobiol., A* **1999**, *128*, 101−109.
(28) Hollins, B.; Noe, B.; Henderson, J. M. *Clin. Chem.* **1987**, *33*, 765−768.
(29) Devoisselle, J. M.; Soulie-Begu, S.; Mordon, S.; Desmettre, T.; Maillols, H. *Lasers Med. Sci.* **1998**, *13*, 279−282.
(30) Mordon, S.; Devoisselle, J. M.; Begu, S.; Desmettre, T. *Lasers Med. Sci.* **1998**, *13*, 181−188.
(31) Yuan, B. H.; Chen, N. G.; Zhu, Q. *J. Biomed. Opt.* **2004**, *9*, 497−503.
(32) Saxena, V.; Sadoqi, M.; Shao, J. *Int. J. Pharm.* **2004**, *278*, 293−301.
(33) Saxena, V.; Sadoqi, M.; Shao, J. *Int. J. Pharm.* **2006**, *308*, 200−204.
(34) Saxena, V.; Sadoqi, M.; Shao, J. *J. Photochem. Photobiol., B* **2004**, *74*, 29−38.
(35) Angelatos, A. S.; Radt, B.; Caruso, F. *J. Phys. Chem. B* **2005**, *109*, 3071−3076.
(36) Skirtach, A. G.; Antipov, A. A.; Shchukin, D. G.; Sukhorukov, G. B. *Langmuir* **2004**, *20*, 6988−6992.
(37) Skirtach, A. G.; Dejugnat, C.; Braun, D.; Susha, A. S.; Rogach, A. L.; Parak, W. J.; Mohwald, H.; Sukhorukov, G. B. *Nano Lett.* **2005**, *5*, 1371−1377.
(38) Skirtach, A. G.; Javier, A. M.; Kreft, O.; Kohler, K.; Alberola, A. P.; Mohwald, H.; Parak, W. J.; Sukhorukov, G. B. *Angew. Chem., Int. Ed.* **2006**, *45*, 4612−4617.
(39) Radt, B.; Smith, T. A.; Caruso, F. *Adv. Mater.* **2004**, *16*, 2184.
(40) Caruso, F.; Caruso, R. A.; Mohwald, H. *Science* **1998**, *282*, 1111.
(41) Caruso, F. *Chem.—Eur. J.* **2000**, *6*.
(42) Rana, R. K.; Murthy, V. S.; Yu, J.; Wong, M. S. *Adv. Mater.* **2005**, *17*, 1145−1150.
(43) Murthy, V. S.; Rana, R. K.; Wong, M. S. *J. Phys. Chem.* **2006**, *110*, 25619−25627.
(44) Yu, J.; Murthy, V. S.; Rana, R. K.; Wong, M. S. *Chem. Commun.* **2006**, 1097.

indocyanine green (ICG, ~90%, Sigma-Aldrich) were used as received. A nitric acid solution (70 wt % HNO_3, Fisher Science) was diluted to 2 wt %. Stock solutions of PAH, Na_2HPO_4, and ICG (1 mg/mL) were prepared using deionized water (18.2 MΩ, Barnstead Nanopure Diamond System) and stored at 4 °C before use. Silicon oxide NPs (13 nm diameter) were available as an aqueous colloidal suspension (20.5 wt %, pH 3.4, Snowtex-O, Nissan Chemicals) and used without further purification. Phosphate buffered saline (PBS) solution (0.01 M PO_4^{3-}, 0.138 M NaCl, 0.0027 M KCl, pH 7.4) was prepared by using premade powder (Sigma-Aldrich).

Synthesis. Nanoparticle-assembled capsules (NACs) were synthesized by combining the PAH solution (2 mg/mL, 20 μL) with the Na_2HPO_4 solution (0.01 M, 120 μL) at room temperature. The ratio of total negative charge of the added salt to the total positive charge of the polymer, or the *R* ratio, was set at 6. The resulting suspension was aged for 10 min at 4 °C, which was then combined and mixed with the SiO_2 sol (diluted to 7 wt %, 60 μL). The resulting NACs were aged for 2 h at 4 °C and washed twice with PBS solution.

IGC containing NACs (ICG-NACs) were prepared by adding the ICG solution (60 μL) of a given concentration (0 to 1.29 mM) to the 10 min aged polymer aggregate suspension and then adding the SiO_2 sol. These concentrations corresponded to precursor molar ratios of ICG to amine monomer units in the range of 0−0.18. The suspension was aged for 2 h at 4 °C, and the capsules were recovered via centrifugation and washed twice with PBS. Unless stated otherwise, the capsules were resuspended in PBS solution. The synthesis of fluorescently labeled ICG-NACs was carried out by replacing PAH with PAH conjugated with FITC (fluorescein isothiocyanate), which was used for confocal microscopy.

Characterization. Fluorescence and bright-field optical microscopy images were obtained using a Leica DM2500 Research Microscope. Laser-scanning confocal microscopy was performed on a Carl Zeiss LSM 510 Meta microscope (laser excitations of 488 and 633 nm for FITC and ICG, respectively). The bandpass filter for FITC had a 500−550 nm range, and for ICG, 650−710 nm. Samples were mounted on conventional glass slides and sealed under a cover slip to prevent drying. All samples were prepared approximately 2−2.5 h prior to imaging, including NAC aging time. Line intensity profiles of ICG-NACs in fluorescence images were collected using ImageJ software.[45] Scanning electron microscopy (SEM) images were performed with FEI XL-30 environmental SEM operating at 30 kV with a working distance of 10.0 mm. The NACs were washed twice, loaded on a SEM stud, dried under air overnight, and sputter-coated with gold before SEM imaging.

Absorbance spectra of ICG-containing solutions and ICG-NAC suspensions were performed using a UV−vis spectrometer (Shimadzu, model UV2401-PC). The samples were handled in a low-light environment to minimize ICG interactions with ambient light. The hydrodynamic diameter of polymer aggregates was characterized through dynamic light scattering (Brookhaven, ZetaPALS with BI-9000AT digital autocorrelator, $\lambda = 656$ nm). The electrophoretic mobility of these aggregates was measured by phase analysis light scattering (PALS) using the ZetaPALS setup. A dip-in (Uzgiris type) electrode system with 4 mL polystyrene cuvettes was used, and measurements were taken at 20 °C.

ICG Loading Efficiency and Content Determination. The amount of ICG loaded into the NACs was determined from the free ICG that was not incorporated inside the NACs. Procedurally, one batch of ICG-NACs was centrifuged and the supernatant was carefully removed and stored in a 15 mL centrifuge tube; the capsules were dispersed in PBS solution. The centrifugation was repeated, and the collected supernatant was combined with the other supernatant volume. The ICG concentration was quantified via UV−vis spectroscopy. ICG decay was found to be negligible at the ICG concentrations measured, consistent with published reports of ICG stability at high concentrations in water.[46] ICG inside the NACs were also measured to check the accuracy of the above method. Selected samples of ICG-NACs were treated with HNO_3 solution to induce capsule disassembly and ICG release into solution. For all samples tested, the amount of released ICG and unencapsulated ICG equaled the initial precursor ICG, indicating mass balance was closed.

Loading efficiency was calculated as the mass of ICG incorporated by the NACs divided by the total ICG mass added to the polymer aggregate suspension. The loading content was calculated as the mass of ICG incorporated into the NACs divided by the mass of the dried ICG-NACs. Measurements were performed at least 3 times to ensure reproducibility.

ICG Leakage Measurements. The synthesis of ICG-NACs with ICG/PAH = 0.04 was scaled up by 10 times. After washing with PBS solution, the precipitate was dispersed in PBS solution (2.6 mL) and split into 10 0.25 mL aliquots kept under constant shaking in the dark at either 23 or 37 °C. Because of the long time scale of this study and the sensitivity of ICG to degradation in water, the suspension fluid was not analyzed for released ICG. Instead, the ICG contained within the ICG-NACs was quantified by inducing the disassembly of the ICG-NACs and immediately measuring the ICG concentration. Specifically, after a given aging time, each aliquot was centrifuged for 30 min and the concentrated precipitate suspension (500 μL) was combined with 2.5 mL HNO_3 solution (2 wt %). The resulting clear solution was then analyzed through UV−vis spectroscopy. As control samples, fresh ICG solution in PBS was prepared with a concentration close to that of the disassembled NAC solution (~0.04 mg/mL) and incubated at 23 and 37 °C. The samples were kept in the dark during aging.

Laser-Induced Photothermal Experiments. Washed ICG-NACs (0.5 mL, $\sim 1 \times 10^7$ particles/mL, $\sim 1 \times 10^9$ ICG molecules/particles, 0.007 wt % ICG of suspension) were suspended in PBS solution and placed in the wells of a 24 well polystyrene culture dish. Control samples were a 0.007 wt % PBS solution of ICG and PBS solution. Containing 0.5 mL of aqueous suspension or solution, each well was irradiated with a continuous-wave near-infrared diode laser (Coherent FAP-System, 54 W, $\lambda = 808$ nm, irradiance (I_o) = 155 W/cm^2) for various time intervals. The laser beam impinged on the sample with a 6.66 mm diameter. During irradiation, the sample temperature was monitored with a K-type thermocouple (bead diameter = 0.003 in., Omega Engineering) located 1 mm outside the laser spot and recorded using LabVIEW data acquisition software (National Instruments, Austin, TX). For the SEM study, 5 identical batches were prepared and irradiated for various times. Each sample was then washed twice with Nanopure water and dried at room temperature for SEM imaging.

Viability Assessment of Cells Exposed to ICG-NACs. Centrifuged ICG-NACs (20 μL, $\sim 1 \times 10^8$ particles/mL, $\sim 1 \times 10^9$ ICG molecules/particle, 0.02 wt % ICG of total suspension) were added to 24-well petri dishes containing cultured fibroblasts (rat maxillary incisor pulp cells (RPC-C2A), incubated in DMEM (Dulbecco's Modified Eagle's Medium) at 37 °C for 1 day; cell density of ~2000 cells/cm^2; 2 mL, growth area of 1.9 cm^2). Per well, the final concentration of ICG-NACs was ~0.0003 wt %, equivalent to final concentrations of 0.00004 wt % ICG, 0.00015 wt % PAH, and 0.00005 wt % SiO_2 NPs. The ICG-NAC/cell culture

(45) http://rsb.info.nih.gov/ij/; 1.34 ed., 2005.

(46) Saxena, V.; Sadoqi, M.; Shao, J. *J. Pharm. Sci.* **2003**, *92*, 2090−2097.

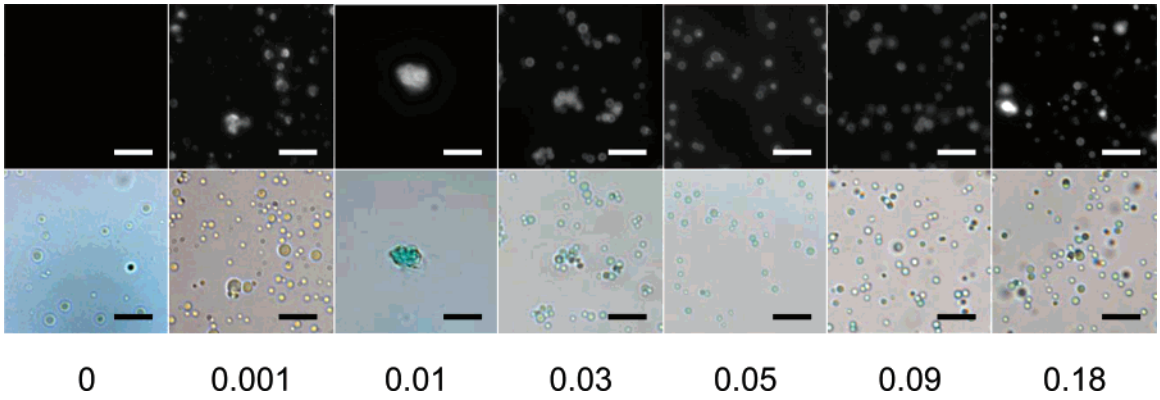

Figure 3. Fluorescence (top row) and bright-field (bottom row) optical images of ICG-containing PAH/phosphate aggregates prepared with various ICG/amine precursor ratios (scale bar = 10 μm).

was incubated at 37 °C for 2 days; four wells were run in replicate. Cell survival was quantified using the Live/Dead viability assay (Molecular Probes). Dead cells were differentiated from live cells through fluorescence microscopy, as the former emitted red fluorescence (from the ethidium homodimer-1 dye precursor) and the latter emitted green fluorescence (from the calcein acetoxymethyl ester dye precursor). Other materials were similarly tested, at final concentrations higher than that of ICG-NACs: PAH solution (20 μL, 2 mg/mL, with a final concentration of 0.002 mg/mL or 0.002 wt %), SiO_2 sol (20 μL, 0.2 wt %, pH 7, with a final concentration of 0.002 wt %), NAC suspension (20 μL, $\sim 10^7$ particles/mL, with a final concentration of $\sim$0.0003 wt %), PBS solution of ICG (0.02 wt %, with a final concentration of 0.0002 wt %), and PBS solution.

Results and Discussion

Synthesis of ICG-Containing NACs. The "encapsulation" of ICG within NACs entails the addition of ICG molecules into the polymer aggregate intermediates before the SiO_2 NPs are added to form the shell. (Encapsulated ICG will be seen to reside within the NAC shell and in the core interior.) This three-step procedure is schematically shown in Figure 2 as pathway (b). After the PAH/phosphate aggregate formation step, ICG was added to the suspension at various ICG/amine monomer precursor ratios. All suspensions were found with polymer aggregates containing ICG, according to fluorescence microscopy visualization (Figure 3). The aggregates were spherical in shape and isolated from one another for most ICG/monomer ratios. There was an intermediate range in which the aggregates formed large clumps, as typified by the suspension prepared with an ICG/amine ratio of 0.01 (Figure 3).

We performed electrophoretic mobility (μ_E) measurements to gain insight into this clumping behavior. Without ICG, the PAH/phosphate aggregates were very positively charged, as indicated by the measured μ_E value of +1.2 (μm/s)/(V/cm) (Figure 4). The electrophoretic mobility decreased in magnitude with increasing ICG/PAH precursor ratio, eventually crossing over to negative values above ICG/amine = 0.018. Suspensions with ICG/amine ratios higher than 0.45 were not analyzed because of excessive laser absorption by the ICG. These results indicate that negatively charged ICG molecules interact electrostatically with the positively charged PAH/phosphate aggregates, such that ICG neutralizes the effective polymer aggregate surface charge at a high enough

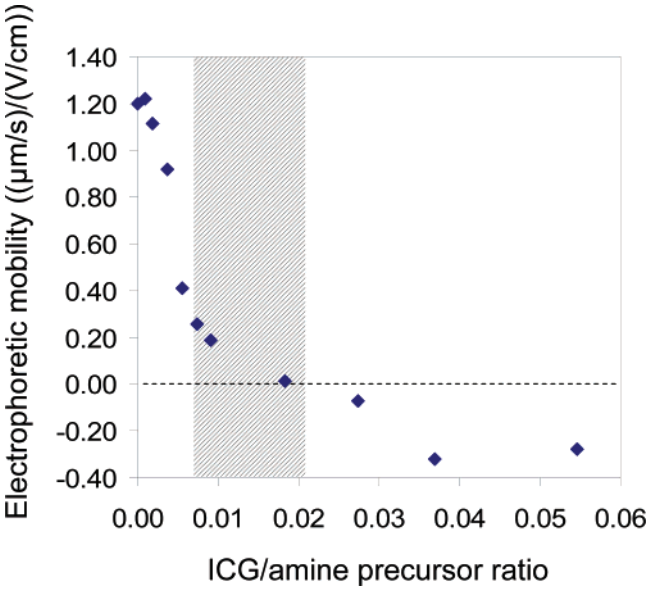

Figure 4. Electrophoretic mobility measurements of ICG-containing PAH/phosphate aggregates prepared with variable amounts of ICG precursor. The undesirable aggregate "clumps" formed in the hatched region. The error for each data point is ±10%.

amount. Additional ICG causes surface charge reversal, suggestive of ICG binding to the polymer aggregate exterior.

The polymer aggregates formed clumps in the ICG/amine range of 0.007 and 0.021, which could be correlated to near-zero μ_E values indicative of near-neutral net surface charge. This correlation is consistent with the well-known DLVO (Derjaguin−Landau−Verwey−Overbeek) theory of colloid stability.[47] Highly charged colloidal particles (whether positively or negatively charged) repel one another electrostatically in suspension to overcome the van der Waals attractive interparticle forces. Weakly charged particles, on the other hand, do not sufficiently repel one another, lowering the energy barrier for particle aggregation (or clumping, in the case of our polymer aggregates) to thermal energy levels. We have used a similar analysis to understand the growth-rate dependence of polymer aggregates on *R* ratios and pH values.[42−44]

The third step of ICG-NAC synthesis was carried out by adding the SiO_2 NP sol to the ICG-containing aggregate

(47) Hunter, R. J. *Foundations of Colloid Science*; Oxford University Press: New York, 2001.

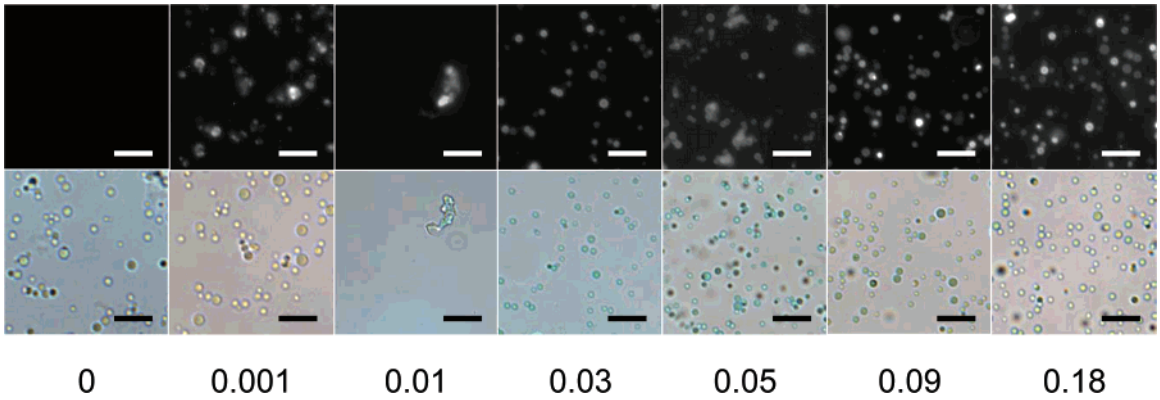

Figure 5. Fluorescence (top row) and bright-field (bottom row) optical images of ICG-containing NACs derived from the PAH/phosphate aggregates (prepared with various ICG/amine precursor ratios) shown in Figure 3 (scale bar = 10 μm).

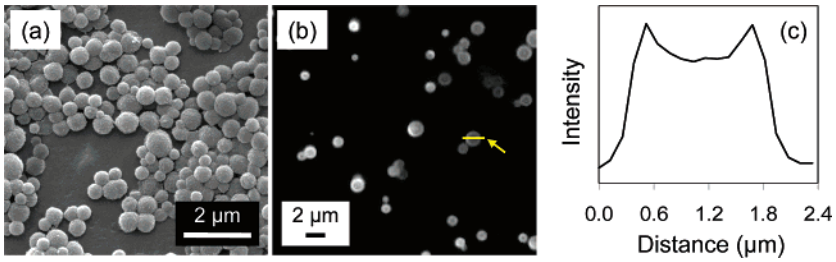

Figure 6. (a) SEM image of dried ICG-NACs, (b) fluorescence image of ICG-NACs in aqueous suspension, and (c) fluorescence intensity line profile of one capsule as indicated in panel (b). The ICG-NACs were prepared with an ICG/amine precursor ratio of 0.04.

suspension (Figure 2). The resulting ICG-NACs assumed the shape and disperse state of the parent aggregates. The sample prepared with an ICG/amine ratio of 0.01 contained ill-defined particles due to the clumping of the polymer aggregates. As in the case of the parent aggregates, there was no apparent trend in capsule size with ICG precursor amount (Figure 5). All the ICG-NACs were roughly 1 μm in diameter, with the largest ones observed with a diameter of 2 μm, and the smallest, 0.6 μm. Dried under vacuum during SEM imaging, the ICG-NACs underwent contraction like the NACs prepared using poly(lysine) instead of PAH,[42] resulting in capsules with diameters less than 1 μm (Figure 6a). They did not fracture or deform after drying, maintaining their spherical shape. In suspension, the ICG-NACs were colloidally stable and did not precipitate even after 6 months. Macroscopically, they appeared as a greenish and cloudy suspension, which could be readily centrifuged to give a green-colored precipitate and a colorless supernatant (Figure 7).

The NACs had loading contents ranging from 0.4 to 23.1 wt % (Table 1). The loading content could be increased by using higher ICG/amine ratios, but the loading efficiency correspondingly decreased (from as high as 97% to as low as 34%). The ICG/PAH ratios between 0.03 and 0.05 were seen as the optimum synthesis range in which loading efficiency and loading content were both high. For comparison, the ICG-containing PLGA particles of Saxena et al. had loading efficiencies as high as 75% and loading contents as high as 0.3 wt %.[32]

Absorbance Properties of ICG-Containing NACs. The absorbance of ICG-NACs were analyzed by considering NACs prepared with an ICG/amine ratio of 0.04. ICG-NACs clearly exhibited absorption in the NIR and partially in the visible range, with an absorbance peak located at 830 nm

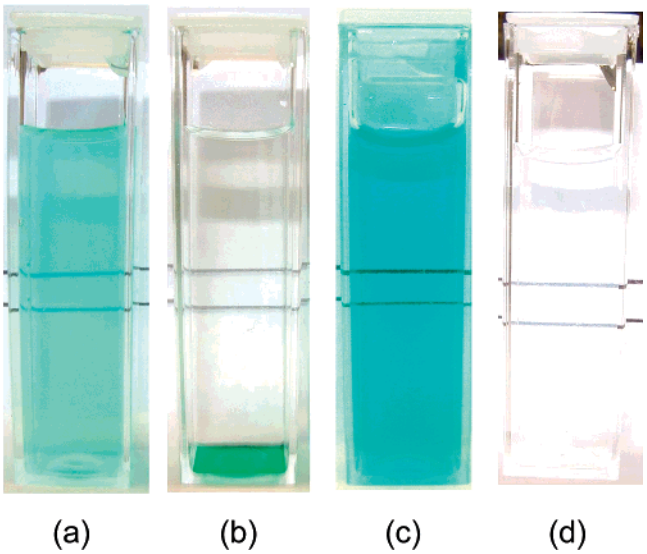

Figure 7. Cuvettes containing ICG-NACs (0.04 mg of ICG/mL, 0.3 mg of ICG-NACs/mL) (a) before and (b) after centrifugation; (c) PBS solution of ICG (0.04 mg/mL); and (d) NACs (0.3 mg of NACs/mL). The double-lines are drawn in the background to aid in observing suspension cloudiness.

and a less intense shoulder at 740 nm (Figure 8a). Light scattering from the suspended NAC particles contributed to a higher background in the absorbance spectrum, as was seen for the case of the non-ICG-containing NAC suspension (Figure 8c). In contrast, an aqueous ICG solution of the same ICG concentration had peaks located at 780 and 700 nm, representing ICG monomers (single ICG molecules) and dimers (aggregates of 2 ICG molecules), respectively (Figure 8b).[10,48] The absorption maxima are known to red-shift to

(48) Holzer, W.; Mauerer, M.; Penzkofer, A.; Szeimies, R. -M.; Abels, C.; Landthaler, M.; Baumler, W. *J. Photochem. Photobiol., B* **1998**, *47*, 155−164.

Table 1. ICG Loading Efficiency and Content of ICG-NACs as a Function of ICG/Amine Precursor Ratio[a]

	ICG/amine ratio						
	0.001	0.03	0.04	0.05	0.07	0.09	0.18
loading efficiency (%)	91.4 ± 4.4	97.1 ± 3.8	95.2 ± 3.4	90.0 ± 2.7	80.6 ± 2.9	65.5 ± 3.2	34.1 ± 2.9
loading content (wt %)	0.4 ± 0.02	11.3 ± 0.4	14.3 ± 0.5	19.2 ± 0.6	22.1 ± 0.8	22.4 ± 1.1	23.1 ± 2.0

[a] Encapsulated ICG will be seen to reside within the NAC shell and in the core interior.

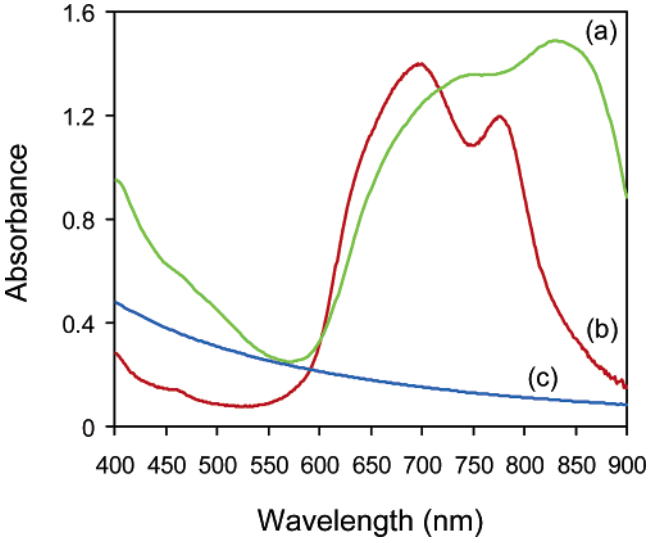

Figure 8. UV−vis absorbance spectra of (a) ICG-NACs prepared at ICG/amine = 0.04 (0.04 mg of ICG/mL, 0.3 mg of ICG-NACs/mL), (b) PBS solution of ICG (0.04 mg/mL), and (c) NACs (0.3 mg of NACs/mL).

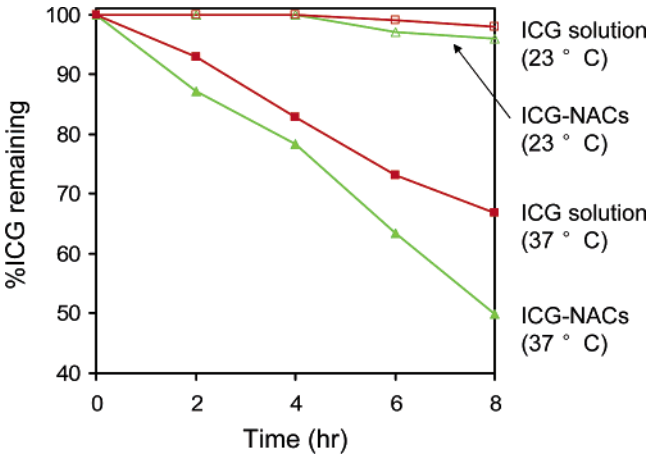

Figure 9. ICG amount remaining in ICG-NACs (prepared at ICG/amine = 0.04; 0.04 mg of ICG/mL, 0.3 mg of ICG-NACs/mL) and in free ICG solution as a function of time, at two different temperatures (23 and 37 °C). The error for each data point is ±5%.

∼805−810 nm when there are albumin and plasma proteins present in solution.[1,10,27,28] This red-shift has been attributed to the strong binding between ICG and protein molecules. These ICG solutions and ICG-containing Intralipid suspensions show some absorbance at 830 nm,[31,49] but an absorbance peak at this wavelength has not been previously reported. We suggest that the 830 and 740 nm peaks represent ICG monomers and dimers binding more strongly to the NACs than to proteins.

ICG molecules appeared to be concentrated in the periphery of both the polymer aggregate intermediates and the resultant NACs (Figures 3, 5, and 6b). Upon closer examination, ICG-NACs were found to fluoresce within the core interior as well (Figure 6c). These data indicate that ICG was encapsulated in the core interior of the NACs and within the shell wall. Confocal analysis of ICG-NACs synthesized with PAH-FITC verified that the capsules were polymer-filled, that is, the PAH filled the interior of the capsule (see the Supporting Information, Figure S1). Thus, ICG was distributed throughout the NAC volume through electrostatic and hydrophobic interactions within the core interior and the shell.

Release of ICG from ICG-Containing NACs. We quantified the ICG content of ICG-NACs (ICG/amine ratio = 0.04) as a function of time by dis-assembling the capsules and measuring the absorbance of free ICG concentration at 780 nm (Figure 9). For ICG-NACs at 23 °C, more than 96% of ICG was retained. The small loss of ICG was partially the result of thermal degradation, as indicated by the small but finite concentration decrease in the amount of ICG solution. At 37 °C, thermal degradation of free ICG was significant, as 34% was lost at the end of 8 h. The half-life of ICG at 37 °C was calculated to be 19 h, consistent with the published half-life of ∼10 h for an ICG concentration of 0.001 mg/mL at 42 °C.[46] In encapsulated form, 51% of the ICG was lost at the end of 8 h. Accounting for the ICG loss due to thermal degradation (34%), we attributed the difference of 17% to ICG leakage from the capsule. The capsules were not broken (see the Supporting Information, Figure S2), suggesting the leakage was through diffusional loss instead of capsule rupture. The extent of leakage could be reduced by synthesizing ICG-NACs using smaller SiO_2 NPs, which would reduce the interstitial gap sizes within the shell wall. Studies are in progress to investigate the effect of encapsulation on ICG thermal stability and the effect of smaller SiO_2 NPs on ICG leakage.

We compare the ICG-NACs with the ICG-containing PLGA particles of Saxena et al.[32] As mentioned earlier, the latter did not contain much ICG (with a reported maximum loading of 0.3 wt %) relative to ICG-NACs (Table 1), and ICG leakage was significant. Specifically, 78% of ICG was lost from the PLGA particles over an 8 h period at 37 °C in PBS, leaving behind ∼0.07 wt % ICG. Under the same conditions, the ICG-NACs prepared with an ICG/amine ratio of 0.04 retained ∼7.2 wt % ICG (Figure 9). ICG loss due to thermal degradation and leakage (<15% at 2 h) is acceptable on the short time scales of photothermal therapies (∼1−2 h).[14]

Photothermal Behavior of ICG-Containing NACs. The ICG-NACs were capable of laser-induced heat generation, with temperatures reaching >80 °C after ∼30 s of laser irradiation (Figure 10a). An ICG solution of comparable concentration had a very similar heating curve, which indicated that entrapment of ICG within the NAC structure

(49) Milstein, A. B.; Oh, S.; Webb, K. J.; Bouman, C. A.; Zhang, Q.; Boas, D. A.; Millane, R. P. *Appl. Opt.* **2003**, *42*, 3081−3094.

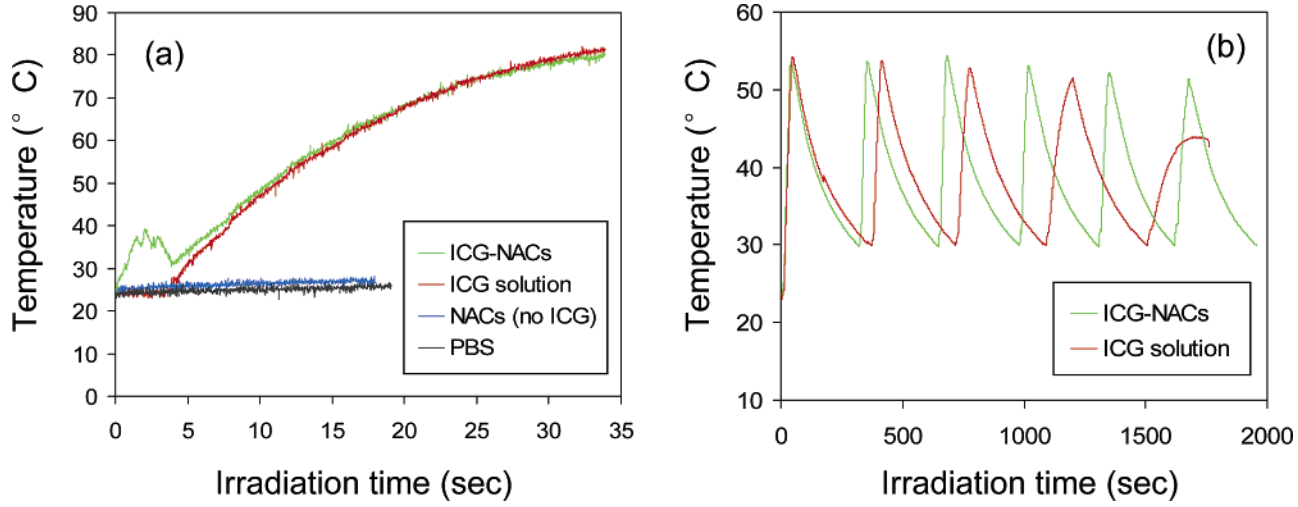

Figure 10. Temperature profiles of ICG-NACs prepared at ICG/amine = 0.09 (0.07 mg of ICG/mL, 0.33 mg of ICG-NACs/mL), PBS solution of ICG (0.07 mg/mL), NACs (0.3 mg of NACs/mL), and PBS solution: (a) constant irradiation to 80 °C, and (b) multiple-cycle irradiation/cooling.

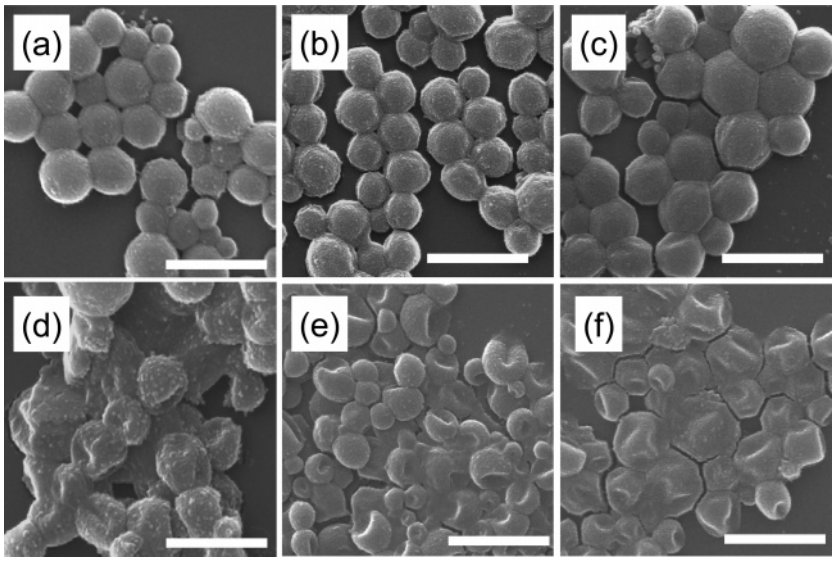

Figure 11. SEM images of ICG-NACs (0.07 mg of ICG/mL) irradiated to different temperatures, under conditions used in Figure 10a: (a) 23, (b) 40, (c) 50, (d) 60, (e) 70, and (f) 73 °C (scale bar = 2 μm).

did not affect its photothermal response. Neither the buffer solution nor the non-ICG-containing NACs contributed to the observed temperature increase. The temperature spikes and heating delay during the first 5 s were experimental artifacts.

These experiments raised the question of NAC thermal stability during irradiation. We analyzed the capsules after various irradiation times through SEM (Figure 11), finding that the ICG-NAC structure was mostly unaffected at 50 °C and lower. They were still spherical but the shell appeared to have some surface restructuring. At 60 °C and higher, the capsules experienced significant structural deformation. The temperature sensitivity of the NAC shell comes from the increased thermal energy with respect to the electrostatic interactions that hold the NPs and the polymer chains together in the shell, i.e., the shell structure "loosens" at higher temperatures. With decreased mechanical strength of the shell, the observed morphological change could have resulted during photothermal heating or during SEM sample preparation. The transition temperature for the thermal stability of ICG-NACs appeared to be 50 °C.

A further comparison of the ICG-NACs and free ICG was made by performing several cycles of photothermal heating and cooling (Figure 10b). Each sample was irradiated until its temperature reachedthe range of ~51−54 °C, after which the samples were allowed to cool to 30 °C before repeating the irradiation. The photothermal heating patterns were found to be quite different. The ICG solution underwent 4 irradiation/cooling cycles before the 51 °C temperature clearly became unreachable, as a result of photodegradation of the ICG molecules. Photodegradation leading to ICG loss may be due to the high temperatures generated or the direct photoinduced decomposition. On the fourth cycle, the temperature increase was noticeably less steep than the earlier cycles and a longer irradiation time was needed to reach 52 °C, indicating the ICG degradation became significant. In contrast, ICG-NACs were able to reach 55 °C for at least six cycles, with little change in the heating profiles. Thus, NAC encapsulation increases the stability of ICG against photodegradation.

The ICG-NACs present an interesting contrast to two other types of NIR-absorbing colloids, especially in terms of ease

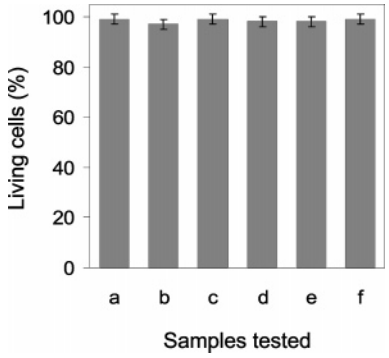

Figure 12. Viability testing of precursors (a) PAH solution, (b) SiO2 NP sol, and (c) PBS solution of ICG and capsules (d) non-ICG-NACs and (e) ICG-NACs. (f) PBS solution is a control sample.

of synthesis. Caruso and co-workers reported the layer-by-layer preparation of micrometer-sized capsules composed of six alternating layers of poly(styrene sulfonate) (PSS) and PAH, a layer of gold NPs, and an outer layer of PSS.[35] The layer-by-layer preparation took at least 6 h, compared to the three-step ICG-NAC preparation (Figure 2b), which took less than 2.5 h (including a 2 h aging period). Gold nanoshells are silica particles coated with a thin shell of gold, and they have optical absorbance maxima in the NIR range that can be tuned with nanometer-scale shell thickness.[50−52] Their preparation is straightforward but requires the careful synthesis of uniform ~100 nm silica particles via the Stöber process (overnight reaction[53]), amine surface functionalization (overnight reaction, 1 h boiling, and 5 times washing via centrifugation[53]), gold NP synthesis (2−3 weeks of aging time[54]), attachment onto the silica surface (30−90 min[53]), and reduction of gold salt to form a complete shell. Halas, West, and co-workers demonstrated that these materials have excellent NIR photothermal properties for potential in vivo laser therapies. It is noted that the gold nanoshells are not encapsulation agents like NACs and layer-by-layer capsules.

Viability of Cells Exposed to ICG-Containing NACs. We studied the biocompatibility of the ICG-NACs by incubating them with fibroblast cells at 37 °C for 2 days. At the concentrations tested, the ICG-NACs were found to be nontoxic, as were the PAH polymer, silica NPs, ICG, and non-ICG-containing NACs (Figure 12). Recalling that the silica NPs are amorphous, these results are consistent with various studies that indicate that amorphous silica powders and NPs are nontoxic, especially compared to crystalline silica.[55−58] Thus, NACs and ICG-NACs are not expected to be toxic materials for in vivo animal studies and clinical applications, although detailed toxicity studies would be required to verify this point.

Conclusions

Stable aqueous suspensions of ICG-containing silica/polymer capsules were synthesized easily through a three-step mixing process at room temperature and in water. The conditions for ICG incorporation were established. Specifically, there was an ICG/polymer ratio range outside of which ICG-NACs could be synthesized with controllable ICG content. Within this range, poorly defined particles were formed as a result of excessive clumping of the ICG-containing PAH/phosphate aggregates, which was attributed to minimally charged aggregate surfaces. At a loading as high as 23 wt % of the total material, the ICG molecules were located within the NP/polymer shell wall and within the polymer aggregate core. Absorbance spectra of ICG-NACs demonstrated that the peak absorption was red-shifted from that of free ICG by ~50 nm. At the physiological temperature of 37 °C, ICG loss from the capsule was due to intrinsic thermal instability of the dye and to leakage. The ICG-containing capsules were active for NIR laser-induced heating, and were more photostable than free ICG. Restructuring of the shells was induced by photothermal heating above 50 °C. The ICG-NACs offer the advantages of high ICG content, minimal leakage compared to other ICG-containing particles, simplicity in preparation (compared to gold-containing, layer-by-layer-assembled capsules and gold nanoshells), and a functionalizable surface, which is important for targeted photothermal therapy. It should even be possible to control the leakage rate at the NP assembly synthesis level by using smaller NPs. The synthesis of ICG-NACs demonstrates a general approach for the nondestructive incorporation of photosensitizers and organic dye compounds.

Acknowledgment. This work was supported by a Smalley-Curl Innovation Award (M.S.W.), a 3M Non-tenured Faculty Award (M.S.W.), NIH GMO-8362 (M.A.Y.), NIH R01-AR47996 (B.A.), and Rice University. We are grateful to Dr. H.-W. Jun and Prof. J. D. Hartgerink for cell cytotoxicity testing, Prof. J. L. West for use of the laser equipment, Dr. P. Diagaradjane for helpful discussions, and to Dr. D. Javier and Prof. R. Richards-Kortum for confocal imaging.

Supporting Information Available: Brightfield and confocal images of ICG-NACs prepared with an ICG/amine precursor ratio of 0.04 and PAH-FITC for FITC and ICG; fluorescence and brightfield images of ICG-NACs (0.04 mg of ICG/mL) after incubating at 37 °C for 8 h. This material is available free of charge via the Internet at http://pubs.acs.org.

CM062080X

(50) West, J. L.; Halas, N. J. *Annu. Rev. Biomed. Eng.* **2003**, *5*, 285−292.
(51) Loo, C.; Lin, A.; Hirsch, L.; Lee, M. H.; Barton, J.; Halas, N.; West, J.; Drezek, R. *Technol. Cancer Res. Treat.* **2004**, *3*, 33−40.
(52) Oldenburg, S. J.; Averitt, R. D.; Westcott, S. L.; Halas, N. J. *Chem. Phys. Lett.* **1998**, *288*, 243.
(53) Westcott, S. L.; Oldenburg, S. J.; Lee, T. R.; Halas, N. J. *Langmuir* **1998**, *14*, 5396−5401.
(54) Gobin, A. M.; O'Neal, D. P.; Watkins, D. M.; Halas, N.; Drezek, R. A.; West, J. *Lasers Surg. Med.* **2005**, *37*, 123.
(55) *Silica, Some Silicates, Coal Dust and Para-aramid Fibrils*; IARC Monographs on the Evaluation of Carcinogenic Risks to Humans; IARC Press: Geneva, Switzerland, 1997; Vol. 68.
(56) http://www.epa.gov/fedrgstr/EPA-PEST/2002/May/Day-15/p11743.htm 2002.
(57) Elias, Z.; Poirot, O.; Daniere, M. C.; Terzetti, F.; Marande, A. M.; Dzwigaj, S.; Pezerat, H.; Fenoglio, I.; Fubini, B. *Toxicol. in Vitro* **2000**, *14*, 409−422.
(58) Brunner, T. J.; Wick, P.; Manser, P.; Spohn, P.; Grass, R. N.; Limbach, L. K.; Bruinink, A.; Stark, W. J. *Environ. Sci. Technol.* **2006**, *40*, 4374−4381.